### Surface-Adsorbed CO as an Infrared Probe of Electrocatalytic Interfaces

Charuni M. Gunathunge, Jingyi Li, Xiang Li, and Matthias M. Waegele\*

Department of Chemistry, Merkert Chemistry Center, Boston College, Chestnut Hill, Massachusetts 02467, United States

E-mail: waegele@bc.edu

#### Introduction

Electrocatalytic interfaces enable chemical transformations of fundamental and technological significance that are challenging to achieve by other means. Examples include the selective oxidation of alcohols, 1,2 the conversion of biomass, 3,4 and the reduction of carbon dioxide, <sup>5,6</sup> and nitrogen. <sup>7,8</sup> However, electrocatalysis of these reactions suffers from poor product selectivity and catalyst deactivation. Addressing these issues requires a better molecularlevel understanding of these complex interfaces (Figure 1). On the electrode side, the electrode material and surface morphology determine the ensemble of catalytically active sites.<sup>5,9-12</sup> On the electrolyte side, key factors that determine the catalysis include the distribution of excess ions in the electric double layer, <sup>13–15</sup> the pH in the vicinity of the electrode, 16-20 the structure of interfacial water, 21,22 and the coverages of surface intermediates and adsorbed electrolyte ions. 14,23 The electrolyte side of the interface couples in intricate ways to the electrode and often evolves the surface morphology under reaction conditions. 24-26 Therefore, in situ and operando techniques are necessary to assess the surface morphology in the electrochemical environment.

Probing the interface under operating conditions is a great experimental challenge. A variety of X-ray techniques, <sup>27,28</sup> surface-enhanced Raman spectroscopy (SERS), <sup>6,29</sup> and surface-enhanced infrared absorption spectroscopy

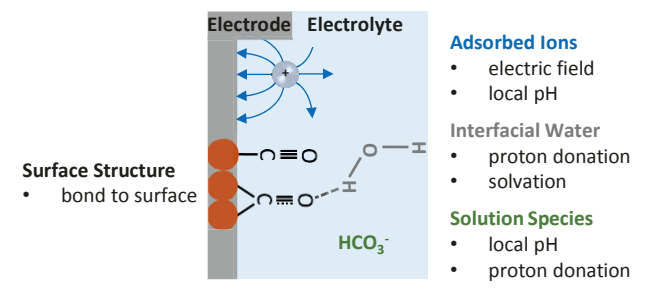


Figure 1: The catalytic activity of the interface is determined by the electrode surface, electrolyte species, and their interplay.

(SEIRAS)<sup>30–32</sup> have emerged as particularly useful methods. While each of the techniques has its strengths and weaknesses, they often provide complementary information. Key strengths of SEIRAS are its high sensitivity, enabling the collection of a spectrum within a few seconds, and its broad spectral window, permitting the simultaneous observation of multiple interfacial species. In this technique, the interaction of incident IR radiation with a nanostructured metal surface gives rise to a plasmonic enhancement of the local IR field in the vicinity of the surface. 33,34 As a result, IR absorption signals from surface-adsorbed species are typically enhanced by factors of 10<sup>1</sup>-10<sup>2</sup> for rough metal films  $^{33,34}$  and  $10^4$ - $10^5$  for nanoscale antennas. 35,36 These enhancements enable the detection of sub-monolayer coverages of adsorbates. The field enhancement steeply decays with increasing distance from the surface, typically within  $\sim 5$  nm,  $^{33,34}$  thereby minimizing contributions from bulk electrolyte species.

SEIRAS is particularly powerful when it is coupled to a suitable molecular probe of the interface. The C≡O stretch mode of surfaceadsorbed CO (CO<sub>ads</sub>) is sensitive to the applied potential, surface morphology, and electric double layer structure.  $\mathrm{CO}_{\mathrm{ads}}$  is an intermediate in the reduction <sup>37</sup> and oxidation of carbon monoxide<sup>38,39</sup> and can be introduced as a spectator species during other reactions. Therefore, it is a powerful and broadly applicable IR probe of the electrocatalytic interface. The utility of CO<sub>ads</sub> for studying the surface morphology of catalysts at the solid/gas interface has long been recognized. 40-42 However, the complex dependence of the C≡O stretch spectra on the local environment of the CO<sub>ads</sub> probe renders the interpretation of the spectra a non-trivial task.

This *viewpoint* is a tutorial on how to infer key structural features of electrocatalytic interfaces from IR spectra of CO<sub>ads</sub>. This tutorial is primarily based on recent experimental work from our laboratory; it is not our goal to provide a review of SEIRAS studies, which were comprehensively surveyed in recent review articles. 30-32 However, for completeness of this tutorial, this article also includes brief descriptions of discoveries made by others on the adsorption of CO on transition metals and the dependence of the  $C \equiv O$  stretch frequency on the character of the adsorption site. We focus on the reductions of CO and CO<sub>2</sub> to hydrocarbons on Cu electrodes. In these processes, CO<sub>ads</sub> is a key reaction intermediate; its reduction corresponds to the rate-determining step in the formation of hydrocarbons. 37,43,44 Therefore, the CO and  $CO_2$  reduction reactions ( $CO/CO_2RR$ ) on Cu electrodes are ideally suited for gaining insights into how the interfacial structure and dynamics control the reaction selectivity.

# Adsorption of CO on Transition Metals

The adsorption of CO on metal surfaces is often thought to arise from a synergistic effect involving the donation and back-donation of charge between CO and metal. <sup>45–48</sup> In a simplistic frontier molecular orbital (FMO) descrip-

tion, the surface bond arises from the transfer of charge from the  $5\sigma$  orbital of CO to the metal and the concurrent donation of charge from the metal to the  $2\pi^*$  orbital of CO (back-donation). The d-band model of Hammer, Morikawa, and Nørskov (HMN model) successfully predicts periodic trends in the adsorption of CO in an atop configuration (CO<sub>atop</sub>) on transition metals. 49,50 According to this model, the surface bond is formed due to the interaction of the FMOs of CO with the sp and d states of the metal. The hybridization energy of the FMOs with the d states of the metal is primarily responsible for the variation of the adsorption energy across different transition metals and adsorption sites.

Although the HMN model is successful in the prediction of periodic trends in the adsorption energy of CO<sub>atop</sub>, it is important to note that xray emission spectroscopy (XES) and ab initio calculations have shown that the formation of the surface bond is accompanied by changes in the electronic structure of the CO molecule beyond the FMOs. 47,48,51-53 The adsorption process involves re-hybridization of the entire  $\pi$ system of the CO molecule. For *late* transition metals, the interaction of the  $\sigma$  system with the states of the metal is often found to be energetically unfavorable due to Pauli repulsion. On the basis of such studies, Föhlisch and co-workers suggested that the net adsorption energy is the net result of  $\pi$  bonding and  $\sigma$  repulsion. <sup>51–53</sup> A more detailed discussion of these models is given in Note 1 of the Supporting Information.

The foregoing discussion shows that the adsorption of CO on transition metals is associated with substantial changes in the electronic structure of the molecule. These changes weaken the intramolecular CO bond. The degree of bond weakening depends on the metal and the geometry of the adsorption site. For this reason, the  $C\equiv O$  stretch frequency of  $CO_{ads}$  is a molecular probe of the atomic-level morphology of the catalyst surface.

The C $\equiv$ O stretch frequency of CO<sub>ads</sub> generally decreases with increasing coordination of the adsorbate by surface metal atoms. At the gas/solid interface CO<sub>atop</sub> is typically observed in the range of  $\sim 2130\text{-}2000~\text{cm}^{-1}$ , whereas

bridge-bonded CO ( $\mathrm{CO}_{\mathrm{bridge}}$ ) is observed in the range of  $\sim\!2000\text{-}1650~\mathrm{cm}^{-1}.^{54}$  For  $\mathrm{CO}_{\mathrm{atop}}$ , the C $\equiv\!\mathrm{O}$  stretch frequency also depends on the coordination of the adsorption site by neighboring surface metal atoms. The dependence of the frequency on the adsorption site geometry can be complex. An expanded discussion is provided in Note 2 of the Supporting Information.

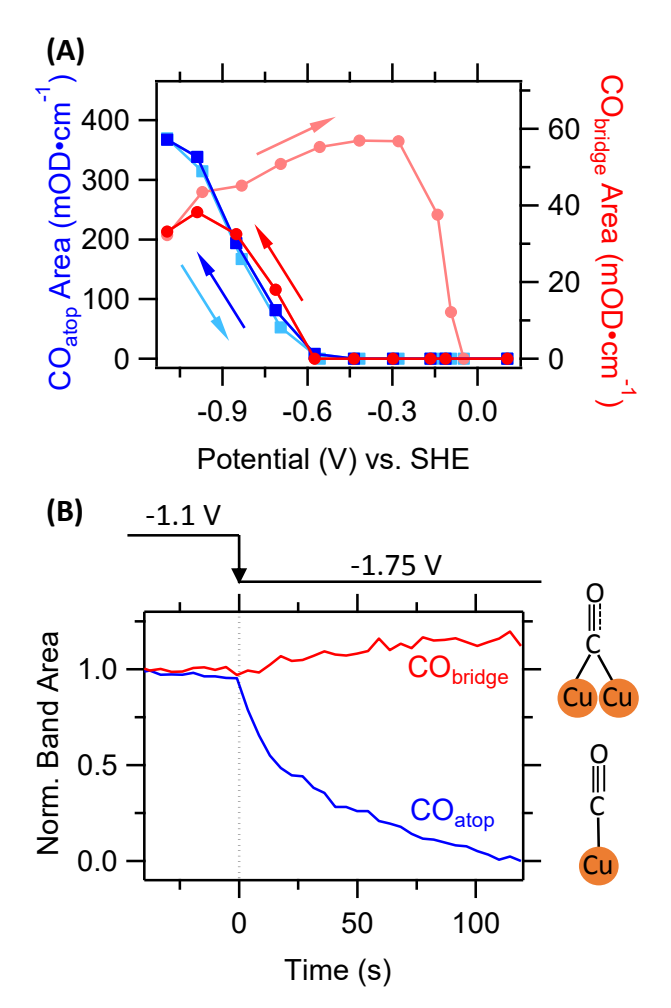


Figure 2: (A) Integrated C $\equiv$ O stretch band areas for CO<sub>atop</sub> (squares) and CO<sub>bridge</sub> (filled circles) during a cyclic voltammetric sweep. CO<sub>bridge</sub> does not desorb on the reverse scan until the oxidation potential of Cu ( $\sim$ -0.15 V) is reached. (B) Response of the integrated band areas for the two species to a cathodic potential step from -1.1 to -1.75 V versus SHE. The CO<sub>bridge</sub> population does not decline. The experiments were carried out in CO-saturated 0.05 M Li<sub>2</sub>CO<sub>3</sub> (pH = 11.4) electrolyte. Panel (A) was adapted from Reference 55.

#### In Situ Probing of Catalyst Surface Morphologies

Rough Cu electrodes often display high CO and CO<sub>2</sub> reduction rates and good product selectivity towards desirable hydrocarbons and oxygenates in comparison with their smooth counterparts. 56-60 However, probing their atomiclevel surface morphology and identifying the catalytically active sites under electrochemical conditions is experimentally very challenging. As a result, the origins of the favorable catalytic properties of these electrodes are still under debate. The following examples demonstrate that the  $C \equiv O$  stretch mode of  $CO_{ads}$  is a powerful in situ probe of the atomic-level morphology and its evolution during catalysis. The technique could therefore provide critical insights required for settling these debates.

The identification of the ensemble of catalytically active sites is of central interest in the field of heterogeneous catalysis. CO<sub>ads</sub> has been generally considered a reactive on-pathway intermediate in the aqueous electrocatalytic reduction of CO<sub>2</sub> on Cu electrodes. However, because the electronic structure of adsorbed CO is dependent on the adsorption site, 47,48,52,61,62 CO<sub>atop</sub> and CO<sub>bridge</sub> are expected to exhibit different surface reactivity. With SEIRAS, we determined the reactivity of CO<sub>atop</sub> and CO<sub>bridge</sub> on a polycrystalline Cu electrode in contact with alkaline electrolytes.<sup>55</sup> The C≡O stretch band of CO<sub>bridge</sub> appears in the spectral range  $\sim$ 1800-1900 cm<sup>-1</sup>. In collaboration with the Janik group, we showed with density functional theory (DFT) calculations that this band is consistent with CO adsorbed on 2-fold and/or 3-fold bridging sites on Cu(100) and Cu(111), respectively. The band likely arises from a mixture of  $\mathrm{CO}_{\mathrm{bridge}}$  species; a contribution from CO<sub>bridge</sub> on other facets is also probable.<sup>63</sup>

Our key findings are as follows: First, we showed that  $CO_{bridge}$  is an irreversibly adsorbed species that can only be removed from the electrode by oxidizing the surface (Figure 2A). Second, we found that  $CO_{bridge}$  cannot be reduced at a potential of -1.75 V versus the standard hydrogen electrode (SHE) (Fig-

ure 2B). Our results suggest that CO<sub>bridge</sub> is not an on-pathway intermediate in CO reduction. With DFT calculations performed by the Janik group, we found that the electrochemical inertness is likely due to a stabilization of CO<sub>bridge</sub> by the interfacial electric field. Third, we extensively explored the electrochemical conditions that lead to a buildup of CO<sub>bridge</sub> on the surface. We discovered that a pH- and potentialinduced surface reconstruction of Cu electrodes forces CO<sub>atop</sub> into a bridge-bonded adsorption configuration. Specifically, we found that the formation of CO<sub>bridge</sub> is favored with increasing pH of the electrolyte. We suggested that under high pH conditions and cathodic polarization, the elemental polycrystalline Cu surface undergoes reconstruction that yields a surface that is more favorable for binding CO in a bridging configuration. This interpretation is consistent with the observation by Soriaga and co-workers that polycrystalline Cu electrodes form (111) and (100) facets on a timescale of tens of minutes under similar electrochemical conditions. <sup>64</sup>

More recently, the site preference of CO<sub>ads</sub> on Cu under electrocatalytic conditions has received close attention. Wu and co-workers explored the appearance of CO<sub>bridge</sub> on differently prepared Cu electrodes under CO<sub>2</sub> reduction conditions. 28 Consistent with our results, they found that CO<sub>bridge</sub> is irreversibly adsorbed on the Cu surface and attributed the accumulation of this species to a surface reconstruction process. However, on the basis of x-ray absorption measurements, they ascribed the reconstruction process to the slow reduction of kinetically stable Cu oxides rather than to the reconstruction of the elemental Cu sur-They found that on electrode surfaces on which Cu(0) predominates, only CO<sub>bridge</sub> appears and neither methane nor ethylene is formed. On electrodes on which Cu(I) predominates, they detected only CO<sub>atop</sub> and the formation of methane. By contrast, on electrodes containing a mixture of Cu(0)/Cu(I), they observed CO<sub>bridge</sub> and CO<sub>atop</sub> and a comparatively high selectivity for methane and ethylene.

The observed correlation between the relative abundance of  $CO_{atop}$  and  $CO_{bridge}$  and the product selectivity raises the question if  $CO_{bridge}$  is

an intermediate, a promoter, or simply a spectator that reports on the surface state of the electrode. Given the stability of CO<sub>bridge</sub> at -1.75 V versus SHE (Figure 2B), we rule out the possibility that CO<sub>bridge</sub> is an on-pathway intermediate, though it could become reactive at more cathodic potentials. CO<sub>bridge</sub> could promote the reaction by stabilizing surface structures that facilitate the CO/CO<sub>2</sub>RR. However, for chemically deposited Cu electrodes, Xu and co-workers found that the adsorption of CO does not affect the reduction of Cu oxides at cathodic potentials.<sup>29</sup> Further, we showed that, within our attainable coverage limits, the presence of CO<sub>bridge</sub> does not affect the adsorption of CO<sub>atop</sub>, 55 which is generally viewed as an on pathway intermediate in the  $CO/CO_2RR$ . When these studies are viewed collectively, it appears that, at low surface coverage, CO<sub>bridge</sub> is best described as an electrochemically inert spectator species that reports on the morphology of the Cu surface.

We further found that, apart from the pH, the appearance of CO<sub>bridge</sub> also depends on the electrolyte's cation and anion. For example, CO<sub>bridge</sub> is particularly prominent in electrolytes containing Cs<sup>+</sup> or Cl<sup>-</sup>. <sup>65,66</sup> These species are known to promote the CO/CO<sub>2</sub>RR to C<sub>2+</sub> hydrocarbons, likely due to electric double layer effects. 14,60,67-69 In addition to these electric double layer effects, these species may also assist in the evolution of the surface to a state that favors the formation of C-C bonds.<sup>5</sup> Further studies are required to determine the surface states that are characterized by CO<sub>bridge</sub> and to quantify to what extent the surface coverage of this species correlates with C-C bond formation rates.

The C $\equiv$ O stretch band of CO<sub>bridge</sub> could be employed as an in situ probe to guide the engineering of electrodes with high reaction selectivity. Indeed, such an approach was recently employed by Sargent and co-workers. They showed that increasing the CO<sub>atop</sub>/CO<sub>bridge</sub> ratio by tuning the electrode properties improves the selectivity for the formation of ethylene. <sup>70</sup> We note in passing that the CO<sub>bridge</sub> species that they detected with SERS presents a stretch band at a higher frequency than that of the

species discussed herein. The higher  $C\equiv O$  stretch frequency (1900-2000 cm<sup>-1</sup>) may be a result of a combination of reasons, such as the use of a differently prepared electrode and different reaction conditions in comparison with those employed in SEIRAS. Finally, in contrast to  $CO_{bridge}$  considered here, CO adsorbed on 4-fold bridging (hollow) sites on Cu(100) was implicated as an on-pathway intermediate to ethylene by IR spectroscopy and DFT studies.<sup>71</sup>

The example discussed above illustrates that dynamic restructuring of catalysts under operating conditions plays an important role in catalysis. Surface reconstructions can be driven by changes in the predominant surface adsorbates. In particular, the adsorption of CO is well known to induce or affect surface reconstruction processes on metal surfaces and electrodes. 72-75 Employing SEIRAS and SERS, we observed the reversible reconstruction of polycrystalline Cu electrodes induced by the adsorption of CO.<sup>25</sup> Our key observations are as follows: First, as shown in Figure 3, the C≡O stretch of  $CO_{atop}$  gives rise to a band at  $\sim 2050$  $cm^{-1}$  at potentials >-1.0 V versus SHE (low frequency band, LFB). At more cathodic potentials, a band at  $\sim 2080 \text{ cm}^{-1}$  develops (high frequency band, HFB). The LFB and HFB are due to CO<sub>atop</sub> on terrace and defect sites, respectively. Second, the Raman spectrum also shows bands at 280 and 360 cm<sup>-1</sup>, which are due to the Cu-CO stretch and the frustrated rotational mode of CO, respectively. The key observation is that these two bands appear virtually concurrently with the HFB (Figure 3). These data suggest that once a certain threshold coverage of CO is reached, the interaction of the adsorbate with the Cu electrode induces a reconstruction of the surface. This reconstruction produces undercoordinated Cu sites, as evidenced by the appearance of the HFB. The emergence of these sites is coupled to the formation of nanoscale features on the surface that bring about a marked enhancement of the surface-enhanced Raman effect, as indicated by the concurrent appearance of the HFB and the bands at 280 and 360  $\text{cm}^{-1}$ . Third, with SEIRAS we showed that the changes in the  $C \equiv O$  band are reversible with potential and

CO surface coverage. This observation suggests that the structural changes in the surface are also reversible.

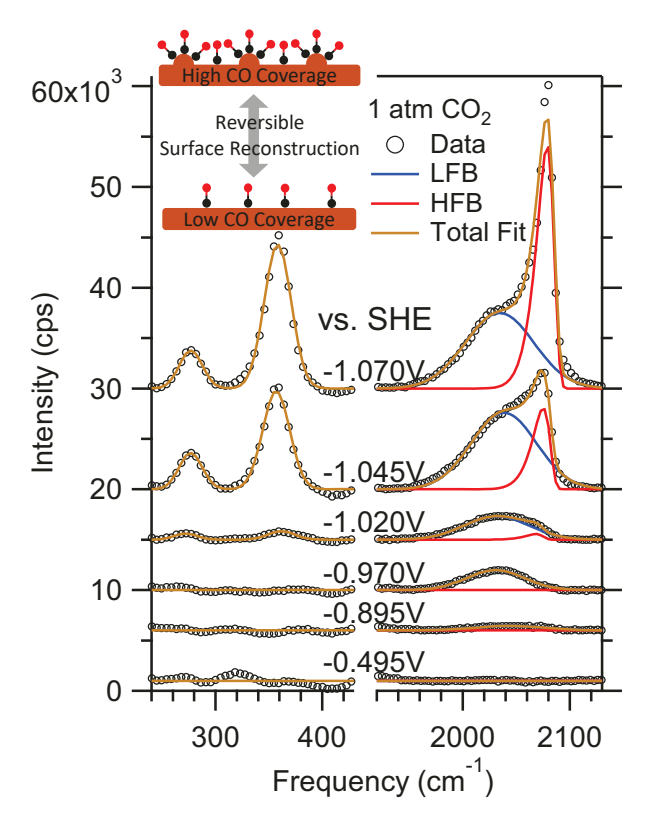


Figure 3: Surface-enhanced Raman spectra of  $CO_{atop}$  during the reduction of  $CO_2$  on a Cu electrode. The concurrent appearance of the  $280/360~\rm cm^{-1}$  bands and the HFB is suggestive of an amplification of the SERS effect due to a CO-induced reconstruction of the surface (cartoon). The red and black solid circles in the cartoon depict the carbon and oxygen atoms of  $CO_{atop}$ , respectively. The data were collected in  $CO_2$ -saturated 0.1 M KHCO<sub>3</sub> electrolyte. Adapted from Reference 25.

Compared with terrace sites, undercoordinated sites bind CO more strongly by about 50-100 meV.  $^{76,77}$  Therefore, the creation of these sites is expected to affect the catalytic properties of the interface. We note that the integrated area of the HFB is not proportional to the population of  $\mathrm{CO}_{\mathrm{atop}}$  on undercoordinated sites; as discussed later, we recently demonstrated that the amplitude of this band is amplified by dynamic dipole coupling.  $^{78}$ 

In a related work, we showed that the reconstruction process is influenced by the identity of the anion of the supporting electrolyte.<sup>66</sup>

Specifically, in 1 M NaClO<sub>4</sub>, we found a hysteresis of  $\sim 100 \text{ mV}$  in the potential-dependent adsorption/desorption profiles of CO<sub>atop</sub> (Figure 4A), indicating that the CO adlayer is more stable on the anodic reverse scan. We and others found similar degrees of hysteresis for a broad range of electrolytes. 66,79,80 Consistent with our prior report, 25 we attributed the higher stability of the CO adlayer on the anodic reverse scan to the CO-induced surface reconstruction that yields undercoordinated Cu sites that bind CO more strongly compared with the prevalent surface sites before reconstruction. Interestingly, in 1 M NaCl, the hysteresis is absent (Figure 4A). This observation suggests that the presence of Cl<sup>-</sup> weakens the binding of CO with the electrode, thereby reducing the degree of CO-induced surface reconstruction. Indeed, we found that the peak frequency of the C≡O stretch band of CO<sub>atop</sub> is markedly blueshifted by  $\sim 19 \text{ cm}^{-1}$  in the presence of 1 M Cl<sup>-</sup> relative to that in 1 M NaClO<sub>4</sub> (Figure 4B). This observation is consistent with the notion of a weakening of the Cu/CO interaction in the presence of this anion.

When they are taken together, our studies discussed above elucidate how the interplay between the Cu surface and CO, anions, and electrolyte pH controls the structural characteristics of the polycrystalline Cu The dynamic nature of the polycrystalline Cu surface highlights the challenges associated with correlating surface morphology with the CO/CO<sub>2</sub>RR activity and product selectivity. To rigorously connect observed product selectivity with surface morphology, it is therefore highly desirable to *simultaneously* perform SEIRAS and product detection on the same electrode. To this end, we developed a combined SEIRAS/differential electrochemical mass spectrometry (DEMS) setup, which we applied to understand the surface morphology and catalytic activity of two types of rough Cu electrodes.

Using our combined SEIRAS/DEMS setup, we established the *potential-dependence* of the *lineshape* of the C $\equiv$ O stretch band of CO<sub>atop</sub> as a probe of the atomic-level surface structure under electrochemical conditions. <sup>78</sup> Our key find-

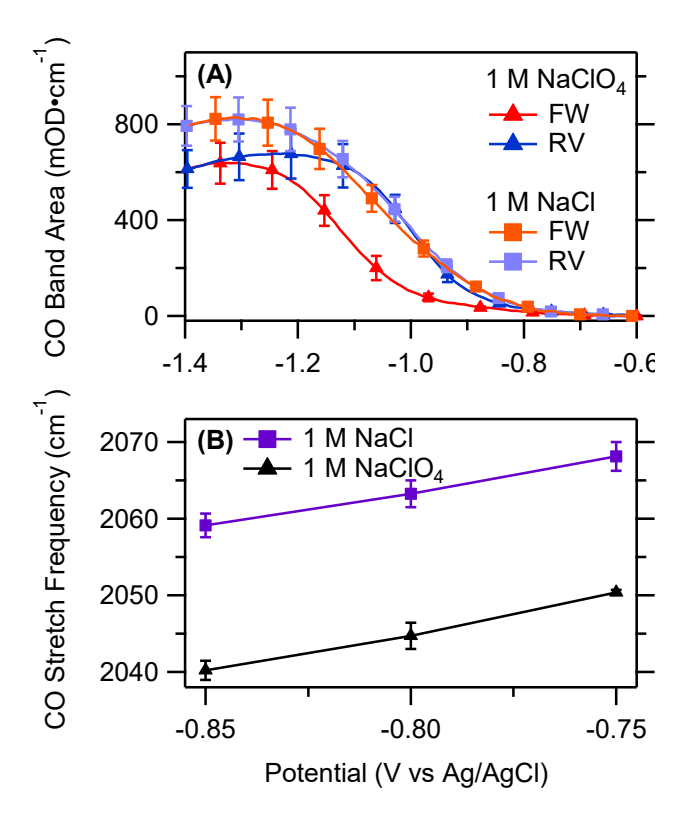


Figure 4: (A) Integrated C $\equiv$ O stretch band areas of CO<sub>atop</sub> on Cu during a cyclic voltammetric sweep in CO-saturated 1 M NaCl and 1 M NaClO<sub>4</sub> in D<sub>2</sub>O, as indicated. "FW" and "RV" denote the forward and reverse scans, respectively. (B) Peak frequency of the C $\equiv$ O stretch band of CO<sub>atop</sub> in the two different electrolyte in the limit of low CO coverage. Adapted from Reference 66.

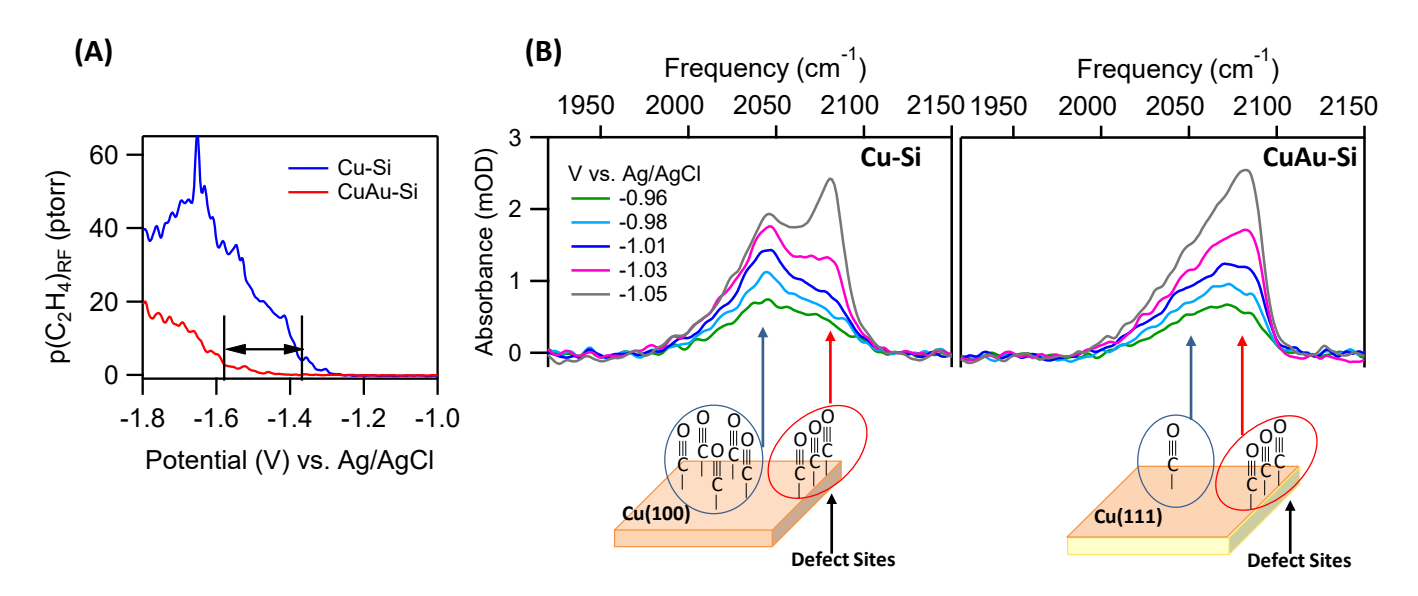


Figure 5: (A) Ethylene formation as determined by DEMS. (B) Lineshape analysis reveals different predominant surface facets on the two types of electrodes. The prevalence of (100) facets on Cu-Si explains the lower overpotential for the formation of ethylene compared with that for CuAu-Si, which is rich in (111) facets. The data were collected in CO-saturated 0.1 M potassium phosphate buffer (pH = 7). Adapted from Reference 78.

ings are as follows: First, we found that Cu films that are electrochemically deposited on Si-supported Au films (CuAu-Si) are not as effective in promoting the formation of ethylene during the reduction of CO in comparison with Cu films (Cu-Si) that are electrolessly deposited onto Si crystals. Specifically, we showed that the onset potential for ethylene is shifted in the cathodic direction by  $\sim 200 \pm 65$  mV for CuAu-Si relative to that for Cu-Si (Figure 5A). Second, the potential-dependence of the lineshape of the  $C\equiv O$  stretch mode of  $CO_{atop}$  is remarkably specific to the type of the electrode. For Cu-Si, a distinct band due to CO<sub>atop</sub> on terraces is apparent at  $\sim 2045$  cm<sup>-1</sup> at moderate cathodic potentials (Figure 5B). By contrast, for CuAu-Si, a distinct band at  $\sim 2045$ cm<sup>-1</sup> does not develop at any applied potential. On the basis of a simple Boltzmann model and additional characterization of the surface morphology through cyclic voltammetry, we showed that these observations are consistent with the prevalence of different terrace sites on the two types of electrodes, which explains their distinct catalytic properties (Figure 5B). CuAu-Si is rich in Cu(111) facets, which is a likely result of pseudomorphic growth of the Cu layer on the Au substrate, which has a preferential (111) orientation. Because of the thickness of the Cu layer (~8 nm), electronic effects arising from the underlying Au substrate are likely negligible; however, the possibility of alloying of the two metals cannot be fully excluded. In contrast to CuAu-Si, the Cu(100) facet predominates on Cu-Si. Cu(100) is known to more efficiently catalyze C−C bond formation in comparison with the (111) facet of Cu. <sup>81</sup> Our analysis of the C≡O stretch bands could also be employed in conjunction with SERS, which can probe a wide range of rough metal electrodes.

# Coverage Effects on the CO Adsorption Energy and C≡O Stretch Spectrum

We now turn to the question of how the C $\equiv$ O stretch spectrum of CO<sub>ads</sub> is affected by changes in the CO coverage and the coadsorption of other species. As the CO coverage increases, interactions between CO<sub>ads</sub> molecules give rise to changes in the spectrum and the adsorption energy. For the purpose of the following dis-

cussion, it is useful to partition the interaction into two terms: (1) Dynamic dipole coupling and (2) all other adsorbate-adsorbate interaction mechanisms.

The theory of dynamic dipole coupling has been extensively described in the literature. 40,82–85 Herein we only describe some of the basic features of the theory. The effects of dynamic dipole coupling are most straightforwardly illustrated for a system involving the interaction of only two CO molecules. The insights are readily extended to a system involving an arbitrary number of CO molecules. Dynamic dipole coupling between two adsorbed CO molecules is given by the following Hamiltonian (in units of cm<sup>-1</sup>):<sup>85</sup>

$$H = \begin{bmatrix} \omega_1 & \beta \\ \beta & \omega_2 \end{bmatrix}, \tag{1}$$

where  $\omega_1$  and  $\omega_2$  denote the frequencies of the CO molecules in the absence of coupling (singleton) and  $\beta$  describes the interaction between the two molecules. The interaction term  $\beta$  can include various coupling effects, depending on the level of theory. Typically,  $\beta$  is taken as a function of the dynamic dipoles  $(\mu)$  of the CO molecules and the distance (r) between a pair of CO molecules, that is,  $\beta = f(\mu_1, \mu_2, r^{-3})$ . For CO, the dynamic dipole  $(\mu)$  is the change in the permanent dipole moment with bond length. Because of the interaction term  $\beta$ , the CO oscillators are no longer isolated, but are coupled to each other. The degree of coupling depends on the distance between the CO molecules and their singleton frequencies. From a practical point of view, it is important to realize that the impact of dynamic dipole coupling on the spectrum greatly depends on the ensemble of adsorption sites, that is, on the surface morphology of the electrode. 40,82,84

We first consider the case where  $\omega_1 = \omega_2$ , which implies that the two CO molecules are adsorbed on identical surface sites. Diagonalization of eq. 1 yields the two normal modes of the coupled system, one with a lower and another with a higher frequency compared with the singleton frequency.<sup>82</sup> The low frequency mode has zero intensity because the two CO molecules oscillate in anti-phase (the amplitude

of an IR band is proportional to the square of total change in dipole moment, which is zero for this mode). By contrast, the high frequency mode, which arises from the two molecules oscillating in-phase, has twice the intensity of the original singleton. Therefore, because the low-frequency mode has zero intensity and only the high-frequency mode is IR active, dynamic dipole coupling between identical CO molecules blue-shifts the frequency. This effect is typically observed for CO adsorbed on low-index single crystal facets where only one type of adsorption site is occupied.<sup>86</sup> The absence of such a shift should not be mistaken for an absence of dynamic dipole coupling: Dynamic dipole coupling is only one interaction mechanism. In a real system, additional adsorbate-adsorbate interactions also affect the frequency, as discussed later. The observed frequency is the net result of the various mechanisms that affect the frequency.  $^{87}$ 

We now consider the case where  $\omega_1 < \omega_2$ , which implies that the two CO molecules are adsorbed on different surface sites. The two normal modes of the coupled system are both IR active. 82 The frequencies of the coupled system are typically very similar to the singleton frequencies. The effect of dynamic dipole coupling primarily manifests itself in the form of intensity transfer from the low to the high frequency mode. 82,84,88 The consequences of this transfer are profound: The transfer effectively amplifies the band of the species that gives rise to the high frequency mode at the expense of the low frequency mode. As a result, minority species (e.g., CO<sub>atop</sub> on defect sites) can dominate the C≡O stretch spectrum, whereas the contribution of the majority species (e.g., CO<sub>atop</sub> on terrace sites) is diminished. Further, when the effects of the metal on the coupling are taken into account, the integrated band area is no longer proportional to the surface coverage (deviation from Beer's law). These effects have been extensively discussed and documented in the literature. 78,82,84,88

Dynamic dipole coupling can be revealed through spectroscopy of isotopically dilute mixtures. 40,82,83 The degree of coupling decreases with increasing difference between the singleton

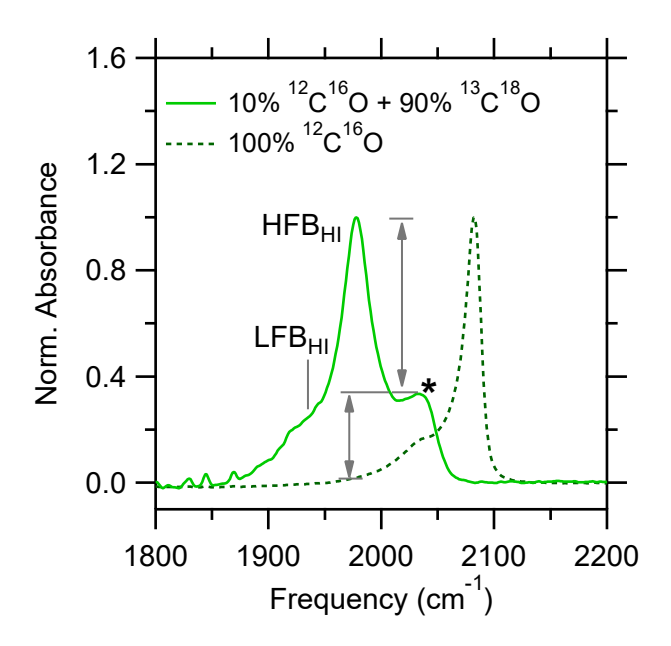


Figure 6: Isotope dillution experiments to reveal dynamic dipole coupling. Spectra were collected at -1.3 V versus Ag/AgCl in pure  $^{12}\text{C}^{16}\text{O}$  and a mixture of 10%  $^{12}\text{C}^{16}\text{O}$  and 90%  $^{13}\text{C}^{18}\text{O}$ . The absence of the HFB of CO in the isotopic mixture indicates that the HFB in the pure  $^{12}\text{C}^{16}\text{O}$  is greatly influenced by the dynamic dipole coupling. The experiments were carried out in 0.1 M potassium phosphate buffer (pH = 7). Adapted from Reference 78.

frequencies ( $|\omega_1 - \omega_2|$ ). As a result, an isotopically dilute CO species shows minimal coupling with the majority CO. An illustrative example is shown in Figure 6. The dashed line shows the  $C\equiv O$  stretch band of  $CO_{atop}$  at saturation coverage. The spectrum consists of two bands, the LFB and HFB, as discussed earlier (Figure 3). The solid line shows the spectrum of an isotopic mixture of 90%  $^{13}C^{18}O$  and 10%  $^{12}C^{16}O$ at the same total coverage and potential. Compared with the spectrum of isotopically pure CO (dashed line), the solid spectrum also shows similar features, denoted LFB<sub>HI</sub> and HFB<sub>HI</sub> (HI is short for "heavy isotope"). These two bands arise from <sup>13</sup>C<sup>18</sup>O. The band labeled with a star symbol primarily arises from <sup>12</sup>C<sup>16</sup>O. Interestingly only the LFB is present; the HFB does not appear. This result demonstrates that the HFB in the spectrum of isotopically pure CO (dashed line) is greatly amplified by intensity transfer from the LFB to the HFB. Clearly, dynamic dipole coupling can complicate the interpretation of spectral lineshapes. However, this mechanism can also give insights into the distribution of CO<sub>ads</sub> on a surface. 86,89

On the basis of this discussion, we recommend the following guidelines for the interpretation of C≡O stretch spectra: First, it is a good default assumption that dynamic dipole coupling occurs within the CO adlayer under many conditions relevant to electrocatalysis. Second, the possible effects of this coupling mechanism for the specific system under consideration should be given thought. As discussed above, intensity transfer is likely to affect the lineshape on polycrystalline electrodes. These effects can be rigorously evaluated with isotopic dilution experiments. 40,82 However, if doubly labeled CO is required (Figure 6), 78 this strategy is prohibitively expensive for typical SEIRAS/SERS measurements. Alternative appropriate control experiments depend on the type of information that is to be extracted from the spectra. These controls may include (1) the analysis of the spectrum in the low coverage limit, where dynamic dipole coupling is weak, unless CO<sub>ads</sub> island formation is favored under the experimental conditions; 86,90 (2) the analysis of the spectra in a potential range of near-constant CO<sub>ads</sub> coverage (if potential-dependent peak frequencies for Stark measurements are of interest, as discussed later); (3) the measurement of additional modes, such as the metal-carbon stretch (Figure 3), which are much less affected by dynamic dipole coupling. Third, when making assignments on the basis of older literature reports, it is good practice to check if the reported assignment held up to further scrutiny. For example, the peak frequency of CO<sub>atop</sub> on Pt(111) was revised because prior results were affected by originally unnoticed surface defects. <sup>91</sup>

Apart from dynamic dipole coupling, the C≡O stretch spectrum of CO<sub>ads</sub> is also affected by other adsorbate-adsorbate interactions. Adsorbates interact by through-space and surface-mediated mechanisms. These mechanisms can be very complex; their review is beyond the scope of this article. In the following, we highlight a few essential points. In contrast to dynamic dipole coupling, these interactions do not only affect the spectrum but also the CO adsorption energy and site preference.

Using DFT calculations, Rappe and coworkers explored the interactions between CO<sub>ads</sub> molecules on various transition metal surfaces. 62 They found that nearest-neighbor interactions weaken the surface bond by  $\sim 0.32$ eV at a coverage of 1/2 monolayers. The degree of weakening is mostly independent of the metal (Pt, Rh, Pd) and adsorption configuration (atop versus bridge sites that do not involve shared surface atoms between different CO<sub>ads</sub> molecules). This interaction is due to through-space repulsion. With increasing coverage of adsorbates, the d-band center of surface metal atoms shifts to more negative energies. 62,92-94 For adsorption configurations in which a surface metal atom binds to more than one CO<sub>bridge</sub> molecule, this shift leads to bonding competition; this effect weakens the interaction of CO with the surface. certain configurations, hybridization between the d-metal orbitals and the  $2\pi^*$  orbitals of CO<sub>bridge</sub> form extended electronic states that facilitate electron delocalization, which stabilizes the CO<sub>bridge</sub> adlayer.<sup>62</sup>

Other coadsorbates may also affect the spectrum and the CO adsorption energy. The in-

teraction of CO with a metal surface is typically strengthened by coadsorption of electron donating species, such as alkali metals. These species increase the charge density on the metal surface, and therefore strengthen the surface bond by increasing the back-donation of charge to the  $2\pi^*$  orbital of  $CO_{ads}$ ,  $^{95,96}$  though favorable through-space electrostatic interactions may also play a role. 97 Consistent with this picture, the C≡O stretch frequency markedly redshifts and bridging sites are preferred over atop sites upon coadsorption of electron-donating species. By contrast, electron-withdrawing coadsorbates, such as sulfur or oxygen, tend to weaken the interaction of CO with the metal.<sup>98</sup>

#### Probing the Electric Double Layer Structure

The electric double layer plays a central role in electrocatalytic reactions. 14,99–102 However, its chemical and physical complexity render the elucidation of the electric double layer structure under reaction conditions very difficult. Further, because of the multitude of different mechanisms through which the electric double layer can influence catalysis, it is very challenging to associate product selectivity with any given measured interfacial property. For these reasons, many studies focus on phenomenological observations or resort to computer simulations to gain insights into electric double layer effects in catalysis. When coupled with a suitable IR probe, vibrational spectroscopy is a powerful tool for the experimental elucidation of electric double layer properties. 103-107 In particular, we are interested in the complex effects of cations on electrocatalytic processes, which we recently reviewed in a perspective article. <sup>14</sup> In the following, we show examples of how spectroscopically measured cation-dependent interfacial properties can be related to the catalytic activity of the interface.

Electric fields at an electrode surface can be probed by the vibrational Stark effect, which describes the effect of an electric field  $(\vec{\mathcal{E}})$  on the frequency  $(\omega)$  of a vibrational mode:

$$\omega(\phi) = \omega_0 - \Delta \vec{\mu} \cdot \vec{\mathcal{E}}(\phi), \tag{2}$$

where  $\omega_0$ ,  $\phi$ , and  $\Delta \vec{\mu}$  are the frequency of the mode in the absence of an electric field, the electrode potential, and the Stark tuning rate of the mode. For  $CO_{ads}$ ,  $\Delta \vec{\mu}$  coincides with the CO bond vector. Detailed accounts of the theory have been given elsewhere. <sup>108,109</sup> Equation 2 enables the calculation of interfacial electric fields in electrocatalytic systems. <sup>22,106,107</sup> It is important to note that the field at the interface is highly heterogeneous. <sup>110</sup> The Stark effect measures the local electric field at the site of the probe projected along  $\Delta \vec{\mu}$  and averaged over the molecular length of the probe molecule.

We explored the effect of alkali metal cations (Li<sup>+</sup>, K<sup>+</sup>, and Cs<sup>+</sup>) on the rate of CO reduction on Cu electrodes. 65 We showed that the CO coverage decreases with increasing size of the alkali metal cation due to the increasing promotion of the hydrogenation of CO<sub>ads</sub> in the series Li<sup>+</sup>, K<sup>+</sup>, and Cs<sup>+</sup>. Specifically, we revealed that the reduction kinetics of CO is faster by approximately one order of magnitude in the presence of Cs<sup>+</sup> compared with that in Li<sup>+</sup>-containing electrolyte. By analysis of the  $C\equiv O$  stretch band of  $CO_{atop}$  we identified the enhanced interfacial electric field in the presence of Cs<sup>+</sup> (compared with Li<sup>+</sup>) as the underlying physical origin of the observed promotion of the CO reduction in Cs<sup>+</sup>-containing electrolyte. Specifically, we found that, with respect of the peak frequency of the C≡O stretch band in Li<sup>+</sup>-containing electrolyte, the frequencies in the presence of K<sup>+</sup> and Cs<sup>+</sup> are shifted to lower energy by about 1.4 and 3.7 cm<sup>-1</sup>, respectively. This observation is consistent with a stronger stabilizing interfacial field with increasing cation size.

To explore electric double layer effects on the reduction of CO to ethylene on Cu, we employed a series of quaternary alkyl ammonium cations (methyl<sub>4</sub>N<sup>+</sup>, ethyl<sub>4</sub>N<sup>+</sup>, propyl<sub>4</sub>N<sup>+</sup>, and butyl<sub>4</sub>N<sup>+</sup>) to systematically tune the properties of the electrocatalytic interface. <sup>22</sup> With DEMS, we revealed that, in the presence of methyl<sub>4</sub>N<sup>+</sup> and ethyl<sub>4</sub>N<sup>+</sup>, ethylene is produced at detectable rates. By contrast, in the pres-

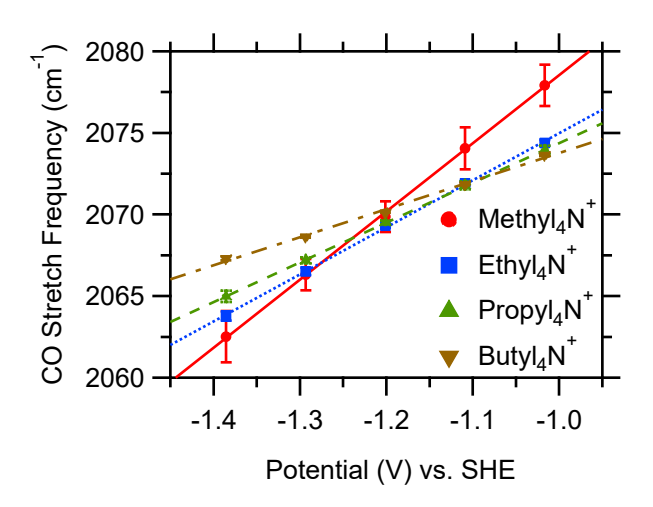


Figure 7: Change of the C $\equiv$ O stretch frequency with applied potential. The experiments were carried out in CO-saturated 0.1 M quaternary alkyl ammonium chlorides in D<sub>2</sub>O, as indicated. Adapted from Reference 22.

ence of propyl<sub>4</sub> $N^+$  and butyl<sub>4</sub> $N^+$ , ethylene is not formed at detectable levels. Using SEIRAS, we comprehensively analyzed how the different cations alter the interfacial properties, including CO coverage, interfacial electric field strength, and the structure of interfacial water. As shown in Figure 7, the slopes of the frequency-potential lines decrease with increasing size of the cation. For the three larger cations, the lines cross at a potential of  $\sim -1.1$ V. The potential is the approximate potential of zero charge of the electrode (the line for methyl<sub>4</sub>N<sup>+</sup> is offset due to chemical effects, as discussed in the original article). At this potential, the interfacial field experienced by CO<sub>atop</sub> is zero. Using this frequency and the Stark tuning rate of CO<sub>atop</sub> on Cu (which is known from calculations), we calculated the potentialdependent interfacial fields. At a potential of -1.6 V versus SHE, we determined that the field strength increases from about 0.05 to 0.15  $VA^{-1}$ . We estimated that these changes do not significantly affect the CO adsorption energy.

Interestingly, our SEIRAS results show that an intermolecular interaction between  $CO_{ads}$  and interfacial water is disrupted in  $propyl_4N^+$ -and  $butyl_4N^+$ -containing electrolytes (Figure 8A). This finding suggests that this intermolecular interaction is essential for the formation of ethylene. In line with a recent

theoretical prediction, <sup>101</sup> we proposed that the waters in direct contact with CO<sub>ads</sub> stabilize the CO dimer, which has been suggested as a key intermediate in the formation of ethylene, <sup>71</sup> through hydrogen bonding (Figure 8B). Our experimental work demonstrates that this non-covalent interaction is critical for the C-C coupling process. At present, the mechanistic understanding of the CO/CO<sub>2</sub>RR is mostly derived from DFT calculations that do not fully include the effects of water. This work highlights the role of water as a solvent in this surface-catalyzed process.

The hydrophobic nature of propyl<sub>4</sub>N<sup>+</sup> and butyl<sub>4</sub>N<sup>+</sup> (compared with the two smaller cations) likely plays an important role in modulating the interaction of water with CO<sub>ads</sub>. However, the rather abrupt change in the rate of ethylene formation with the size of the cation suggests that other effects, such as a high propensity to aggregate at the metal/aqueous electrolyte interface, as observed for some organic cations, 111 may also contribute. Our interpretation is also consistent with the recent observation by Thoi, Hall, and co-workers that cationic surfactants at the electrode/electrolyte interface reorganize interfacial water. 15 As argued by Cuesta and co-workers, the interaction of water with the cation-dependent interfacial electric field likely also plays a role. 112 With vibrational sum frequency spectroscopy (SFG), Dawlaty and co-workers recently showed that on rough Ag electrodes, cationic surfactants produce stronger local electric fields compared with those in the presence of anionic surfactants. 107

#### Conclusions and Outlook

The above examples demonstrate that the C $\equiv$ O stretch band of CO<sub>ads</sub> provides insights into the structural characteristics of the electrode surface and the electric double layer. However, the study of the interface with SEIRAS/CO<sub>ads</sub> is not without pitfalls. It is important to pay particular attention to the points summarized in the following.

SEIRAS Film Integrity. As is the case for

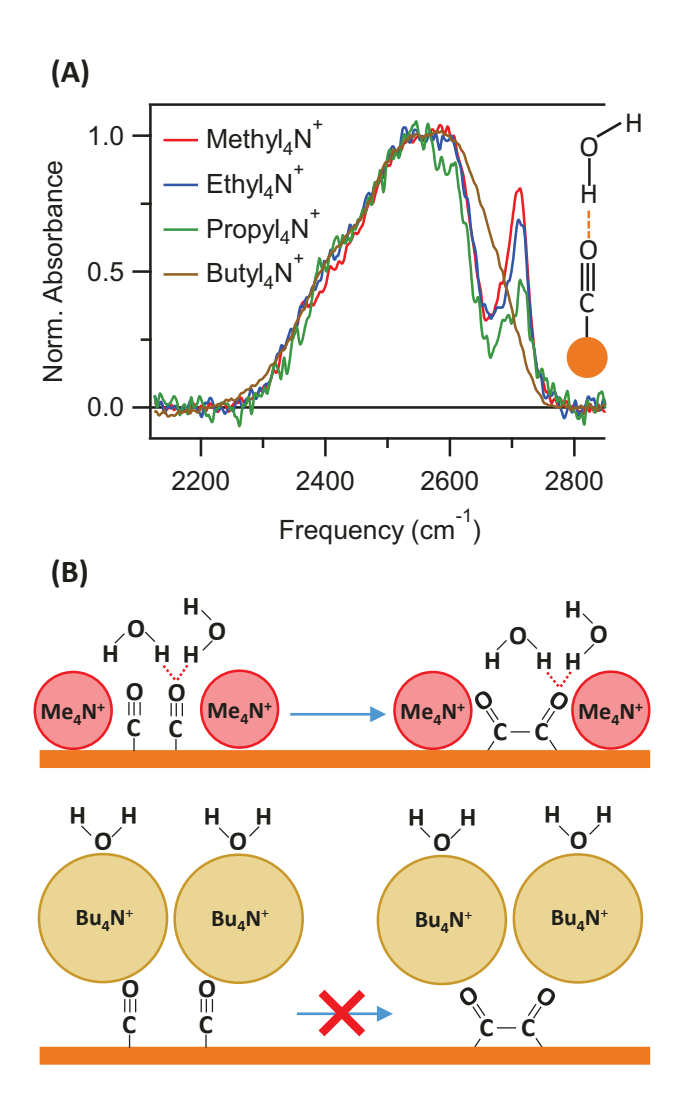


Figure 8: (A) Normalized spectra of O–D band at -1.02 V versus SHE. The experiments were carried out in CO-saturated 0.1 M quaternary alkyl ammonium chlorides in  $D_2O$ , as indicated. The sharp band at  $\approx 2710$  cm<sup>-1</sup> is due to an intermolecular CO-D<sub>2</sub>O interaction. (B) Proposed mechanism. Adapted from Reference 22.

all electrochemical measurements, the preparation and pretreatment procedures of the electrode prior to the measurements may greatly affect the results. Therefore, it is essential to apply appropriate pretreatment protocols and to report those protocols in publications in detail. The proper protocol depends on the thin film electrode's chemistry, the reaction conditions, and the information to be gained from the spectroscopic measurement. For example, the persistence of residual oxide on Cu electrodes can influence the adsorption of CO and the lineshape of the C≡O stretch mode. 113 Proper pretreatment protocols minimize the influence of residual oxides. Whenever possible, it is also advisable to carry out two or more CVs to test if the spectra are impacted by or due to irreversible processes at the interface (e.g., surface reconstructions, pH-drift, etc.).

Reaction Conditions. SEIRAS measurements have often been carried out in static electrolyte and single-compartment cells. a static electrolyte, the pH in the vicinity of the electrode can easily drift under reaction conditions. 18 Further, limited mass transport of other reactants to the surface may also affect the results. 90,114 Because proton-coupled electron transfer reactions are necessarily influenced by pH drifts, appropriate control experiments need to be conducted to ensure that pH effects do not affect the results. Singlecompartment cells may also result in the deposition of trace amounts of counter electrode material on the working electrode. 115 For these reasons, it is advisable to conduct SEIRAS measurements in two-compartment cells and under stirring of the electrolyte. 90 The technical drawings of our SEIRAS two-compartment cell is provided in the Supporting Information. A description of the cell is given in Note 3 of the Supporting Information.

Integration of SEIRAS and Product Detection. When SEIRAS and product detection are carried out separately, it is essential to match the reaction conditions as closely as possible. Compact, two-compartment SEIRAS cells, which can be straightforwardly coupled to gas-chromatography or other product detection systems, are well suited for this purpose.

Flow cells that provide simultaneous probing of the interface with SEIRAS and DEMS provide the tightest integration under well-defined mass transport conditions. <sup>116</sup>

CO Probe. The examples shown herein demonstrate the utility of the C≡O stretch band for probing the interfacial structure. However, for the proper interpretation of the band, close attention has to be payed to coverage effects. It would be desirable to develop additional vibrational probes of the interface that are electrochemically inert over a wide potential range and whose coverage is not potential-The surface coverage of some dependent. nitrile-based probes can be predetermined prior to spectroscopic measurements on some metal Such probes have been proven electrodes. highly successful in the elucidation of the structure of the double layer, <sup>103–105,107</sup> but their limited stability towards reduction limits the use of these probes to moderate cathodic potentials.

Finally, we note that the electric fields extracted from spectroscopic measurements of electrocatalytic interfaces represent the spatially and temporally averaged field within the plane of the electrode. However, the electric field at the electrocatalytic interface is highly heterogeneous, 14,110,117,118 especially if specifically adsorbed ions are present. Surface sites where catalytic turnover occurs may (transiently) experience field strengths very different from the average field. Further advances in spectroscopic methodology and analysis are necessary to characterize the heterogeneity of the field. Using vibrational SFG, Borguet and co-workers recently identified the heterogeneous charge distribution at the aqueous  $\alpha$ -Al<sub>2</sub>O<sub>3</sub> interface. 119 This work suggests that related studies on electrocatalytic interfaces may become possible in the future.

## Supporting Information Available

Expanded discussion on the adsorption of CO on transition metals and the dependence of the C $\equiv$ O stretch frequency on adsorption site geometry. Technical drawings and description of

a two-compartment spectro-electrochemical cell for SEIRAS measurements.

This information is available free of charge on the ACS Publication website.

**Acknowledgement** This work was supported by a CAREER award from the National Science Foundation (Award No.: CHE-1847841). Professor Michael Janik is acknowledged for contributing the DFT calculations on CO<sub>bridge</sub> referenced in this article.

#### Keywords

SEIRAS, surface-adsorbed CO, electrocatalysis, surface-morphology, electric double layer

#### References

- (1) Wang, H.; Jusys, Z.; Behm, R. J. Ethanol Electrooxidation on a Carbon-Supported Pt Catalyst: Reaction Kinetics and Product Yields. J. Phys. Chem. B 2004, 108, 19413–19424.
- (2) Kwon, Y.; Lai, S. C. S.; Rodriguez, P.; Koper, M. T. M. Electrocatalytic Oxidation of Alcohols on Gold in Alkaline Media: Base or Gold Catalysis. J. Am. Chem. Soc. 2011, 133, 6914–6917.
- (3) Lam, C. H.; Lowe, C. B.; Li, Z.; N.; J. T.; Longe, Κ. Rayburn, Caldwell, M. A.; Houdek, С. E.; Maguire, J. B.: Saffron, C. M.: Miller, D. J.; Jackson, J. E. Electrocatalytic Upgrading of Model Lignin Monomers with Earth Abundant Metal Electrodes. Green Chem. 2015, 601 - 609.
- (4) Román, A. M.; Hasse, J. C.; Medlin, J. W.; Holewinski, A. Elucidating Acidic Electro-Oxidation Pathways of Furfural on Platinum. ACS Catal. 2019, 9, 10305–10316.
- (5) Arán-Ais, R. M.; Gao, D.; Roldan Cuenya, B. Structure- and

- Electrolyte-Sensitivity in  $CO_2$  Electroreduction. *Acc. Chem. Res.* **2018**, *51*, 2906–2917.
- (6) Chen, X.: Henckel, D. A.; Nwabara, U. O.; Li, Y.; Frenkel, A. I.; Fister, Т. T.; Kenis, Р. J. Gewirth, A. A. Controlling Speciation during CO<sub>2</sub> Reduction on Cu-Allov Electrodes. ACS Catal. 2020, 672 - 682.
- (7) Hu, L.; Xing, Z.; Feng, X. Understanding the Electrocatalytic Interface for Ambient Ammonia Synthesis. *ACS Energy Lett.* **2020**, *5*, 430–436.
- (8) Lazouski, N.; Chung, M.; Williams, K.; Gala, M. L.; Manthiram, K. Non-Aqueous Gas Diffusion Electrodes for Rapid Ammonia Synthesis from Nitrogen and Water-Splitting-Derived Hydrogen. Nat. Catal. 2020, 3, 463–469.
- (9) Lai, S. C. S.; Lebedeva, N. P.; Housmans, T. H. M.; Koper, M. T. M. Mechanisms of Carbon Monoxide and Methanol Oxidation at Single-crystal Electrodes. *Top. in Catal.* 2007, 46, 320–333.
- (10) Holewinski, A.; Xin, H.; Nikolla, E.; Linic, S. Identifying Optimal Active Sites for Heterogeneous Catalysis by Metal Alloys Based on Molecular Descriptors and Electronic Structure Engineering. Curr. Opin. Chem. Eng. 2013, 2, 312–319.
- (11) Holewinski, A.; Idrobo, J.-C.; Linic, S. High-Performance Ag-Co Alloy Catalysts for Electrochemical Oxygen Reduction. *Nat. Chem.* **2014**, *6*, 828–834.
- (12) Pander, J. E.; Baruch, M. F.; Bocarsly, A. B. Probing the Mechanism of Aqueous CO<sub>2</sub> Reduction on Post-Transition-Metal Electrodes using ATR-IR Spectroelectrochemistry. ACS Catal. 2016, 6, 7824–7833.
- (13) Danilovic, N.; Subbaraman, R.; Strmcnik, D.; Paulikas, A. P.; Myers, D.; Stamenkovic, V. R.; Markovic, N. M. The

- Effect of Noncovalent Interactions on the HOR, ORR, and HER on Ru, Ir, and Ru<sub>0.50</sub>Ir<sub>0.50</sub> Metal Surfaces in Alkaline Environments. *Electrocatalysis* **2012**,  $\beta$ , 221–229.
- (14) Waegele, M. M.; Gunathunge, C. M.; Li, J.; Li, X. How Cations Affect the Electric Double Layer and the Rates and Selectivity of Electrocatalytic Processes. J. Chem. Phys. 2019, 151, 160902.
- (15) Zhang, Z.-Q.; Banerjee, S.; Thoi, V. S.; Shoji Hall, A. Reorganization of Interfacial Water by an Amphiphilic Cationic Surfactant Promotes CO<sub>2</sub> Reduction. J. Phys. Chem. Lett. 2020, 11, 5457–5463.
- (16) Koper, M. T. M. Theory of Multiple Proton-Electron Transfer Reactions and Its Implications for Electrocatalysis. *Chem. Sci.* **2013**, *4*, 2710–2723.
- (17) Varela, A. S.; Kroschel, M.; Reier, T.; Strasser, P. Controlling the Selectivity of CO<sub>2</sub> Electroreduction on Copper: The Effect of the Electrolyte Concentration and the Importance of the Local pH. Catal. Today **2016**, 260, 8–13.
- (18) Yang, K.; Kas, R.; Smith, W. A. In Situ Infrared Spectroscopy Reveals Persistent Alkalinity near Electrode Surfaces during CO<sub>2</sub> Electroreduction. J. Am. Chem. Soc. 2019, 141, 15891–15900.
- (19) Zhang, F.; Co, A. C. Direct Evidence of Local pH Change and the Role of Alkali Cation during CO<sub>2</sub> Electroreduction in Aqueous Media. Angew. Chem. Inter. Ed. 2020, 59, 1674–1681.
- (20) Ryu, J.; Surendranath, Y. Polarization-Induced Local pH Swing Promotes Pd-Catalyzed CO<sub>2</sub> Hydrogenation. J. Am. Chem. Soc. 2020, 142, 13384–13390.
- (21) Remsing, R. C.; McKendry, I. G.; Strongin, D. R.; Klein, M. L.; Zdilla, M. J. Frustrated Solvation Structures Can Enhance Electron Transfer Rates. J. Phys. Chem. Lett. 2015, 6, 4804–4808.

- (22) Li, J.; Li, X.; Gunathunge, C. M.; Waegele, M. M. Hydrogen Bonding Steers the Product Selectivity of Electrocatalytic CO Reduction. *Proc. Natl.* Acad. Sci. U.S.A 2019, 116, 9220–9229.
- (23) Akhade, S. A.; McCrum, I. T.; Janik, M. J. The Impact of Specifically Adsorbed Ions on the Copper-Catalyzed Electroreduction of CO<sub>2</sub>. J. Electrochem. Soc. **2016**, 163, F477–F484.
- (24) Yan, B.; Krishnamurthy, D.; Hendon, C. H.; Deshpande, S.; Surendranath, Y.; Viswanathan, V. Surface Restructuring of Nickel Sulfide Generates Optimally Coordinated Active Sites for Oxygen Reduction Catalysis. *Joule* **2017**, *1*, 600–612.
- (25) Gunathunge, C. M.; Li, X.; Li, J.; Hicks, R. P.; Ovalle, V. J.; Waegele, M. M. Spectroscopic Observation of Reversible Surface Reconstruction of Copper Electrodes under CO<sub>2</sub> Reduction. J. Phys. Chem. C 2017, 121, 12337–12344.
- (26) Medina-Ramos, J.; Zhang, W.; Yoon, K.; Bai, P.; Chemburkar, A.; Tang, W.; Atifi, A.; Lee, S. S.; Fister, T. T.; Ingram, B. J.; Rosenthal, J.; Neurock, M.; van Duin, A. C. T.; Fenter, P. Cathodic Corrosion at the Bismuth-Ionic Liquid Electrolyte Interface under Conditions for CO<sub>2</sub> Reduction. *Chem. Mater.* **2018**, 30, 2362–2373.
- (27) Eilert, A.; Roberts, F. S.; Friebel, D.; Nilsson, A. Formation of Copper Catalysts for CO<sub>2</sub> Reduction with High Ethylene/Methane Product Ratio Investigated with In Situ X-ray Absorption Spectroscopy. J. Phys. Chem. Lett. **2016**, 7, 1466–1470.
- (28) Chou, T.-C.; Chang, C.-C.; Yu, H.-L.; Yu, W.-Y.; Dong, C.-L.; Velasco-Vélez, J.-J.; Chuang, C.-H.; Chen, L.-C.; Lee, J.-F.; Chen, J.-M.; Wu, H.-L. Controlling the Oxidation State of the

- Cu Electrode and Reaction Intermediates for Electrochemical CO<sub>2</sub> Reduction to Ethylene. *J. Am. Chem. Soc.* **2020**, 142, 2857–2867.
- (29) Zhao, Y.; Chang, X.; Malkani, A. S.; Yang, X.; Thompson, L.; Jiao, F.; Xu, B. Speciation of Cu Surfaces During the Electrochemical CO Reduction Reaction. J. Am. Chem. Soc. 2020, 142, 9735– 9743.
- (30) Wang, H.; Zhou, Y.-W.; Cai, W.-B. Recent Applications of in situ ATR-IR Spectroscopy in Interfacial Electrochemistry. Curr. Opin. Electrochem. 2017, 1, 73–79.
- (31) Zhu, S.; Li, T.; Cai, W.-B.; Shao, M. CO<sub>2</sub> Electrochemical Reduction as Probed Through Infrared Spectroscopy. ACS Energy Lett. 2019, 4, 682–689.
- (32) Kas, R.; Ayemoba, O.; Firet, N. J.; Middelkoop, J.; Smith, W. A.; Cuesta, A. In-Situ Infrared Spectroscopy Applied to the Study of the Electrocatalytic Reduction of CO<sub>2</sub>: Theory, Practice and Challenges. *ChemPhysChem* **2019**, *20*, 2904–2925.
- (33) Osawa, M. Dynamic Processes in Electrochemical Reactions Studied by Surface-Enhanced Infrared Absorption Spectroscopy (SEIRAS). *Bull. Chem. Soc. Jpn.* **1997**, *70*, 2861–2880.
- (34) Osawa, M. In Near-Field Optics and Surface Plasmon Polaritons, Topics Appl. Phys.; Kawata, S., Ed.; Springer-Verlag Berlin Heidelberg, 2001; pp 163–187.
- (35) Adato, R.; Yanik, A. A.; Amsden, J. J.; Kaplan, D. L.; Omenetto, F. G.; Hong, M. K.; Erramilli, S.; Altug, H. Ultra-sensitive Vibrational Spectroscopy of Protein Monolayers with Plasmonic Nanoantenna Arrays. *Proc. Natl. Acad. Sci. U.S.A.* **2009**, *106*, 19227–19232.

- (36) Brown, L. V.; Yang, X.; Zhao, K.; Zheng, B. Y.; Nordlander, P.; Halas, N. J. Fan-Shaped Gold Nanoantennas above Reflective Substrates for Surface-Enhanced Infrared Absorption (SEIRA). Nano Lett. 2015, 15, 1272–1280.
- (37) Hori, Y.; Murata, A.; Yoshinami, Y. Adsorption of CO, Intermediately Formed in Electrochemical Reduction of CO<sub>2</sub>, at a Copper Electrode. *J. Chem. Soc.*, Faraday Trans. **1991**, 87, 125–128.
- (38) Samjeské, G.; Komatsu, K.-i.; Osawa, M. Dynamics of CO Oxidation on a Polycrystalline Platinum Electrode: A Time-Resolved Infrared Study. J. Phys. Chem. C 2009, 113, 10222–10228.
- (39) Cabello, G.; Davoglio, R. A.; Marco, J. F.; Cuesta, A. Probing Electronic and Atomic Ensembles Effects on PtAu<sub>3</sub> Nanoparticles with CO Adsorption and Electrooxidation. *J. Electroanal. Chem.* **2020**, 870, 114233.
- (40) Browne, V.; Fox, S.; Hollins, P. Infrared Spectroscopy as an In Situ Probe of Morphology. *Catal. Today* **1991**, *9*, 1–14.
- (41) Eren, B.; Liu, Z.; Stacchiola, D.; Somorjai, G. A.; Salmeron, M. Structural Changes of Cu(110) and Cu(110)-(2×1)-O Surfaces Under Carbon Monoxide in the Torr Pressure Range Studied with Scanning Tunneling Microscopy and Infrared Reflection Absorption Spectroscopy. J. Phys. Chem. C 2016, 120, 8227–8231.
- (42) Wöll, C. Structure and Chemical Properties of Oxide Nanoparticles Determined by Surface-Ligand IR Spectroscopy. *ACS Catal.* **2020**, *10*, 168–176.
- (43) Nie, X.; Esopi, M. R.; Janik, M. J.; Asthagiri, A. Selectivity of CO<sub>2</sub> Reduction on Copper Electrodes: The Role of the Kinetics of Elementary Steps. *Angew. Chem. Int. Ed.* **2013**, *52*, 2459–2462.

- (44) Goodpaster, J. D.; Bell, A. T.; Head-Gordon, M. Identification of Possible Pathways for C-C Bond Formation during Electrochemical Reduction of CO<sub>2</sub>: New Theoretical Insights from an Improved Electrochemical Model. J. Phys. Chem. Lett. 2016, 7, 1471–1477.
- (45) Blyholder, G. Molecular Orbital View of Chemisorbed Carbon Monoxide. *J. Phys. Chem.* **1964**, *68*, 2772–2777.
- (46) Bagus, P. S.; Pacchioni, G. The Contribution of Metal sp Electrons to the Chemisorption of CO: Theoretical Studies of CO on Li, Na, and Cu. *Surf. Sci.* **1992**, *278*, 427–436.
- (47) Dimakis, N.; Cowan, M.; Hanson, G.; Smotkin, E. S. Attraction-Repulsion Mechanism for Carbon Monoxide Adsorption on Platinum and Platinum-Ruthenium Alloys. *J. Phys. Chem. C* **2009**, *113*, 18730–18739.
- (48) Foppa, L.; Copéret, C.; Comas-Vives, A. Increased Back-Bonding Explains Step-Edge Reactivity and Particle Size Effect for CO Activation on Ru Nanoparticles. J. Am. Chem. Soc. 2016, 138, 16655– 16668.
- (49) Hammer, B.; Morikawa, Y.; Nørskov, J. K. CO Chemisorption at Metal Surfaces and Overlayers. *Phys. Rev. Lett.* **1996**, *76*, 2141–2144.
- (50) Chorkendorff, I.; Niemantsverdriet, J. W. Concepts of Modern Catalysis and Kinetics, 2nd, Revised and Enlarged Edition; Wiley-VCH, 2007; pp 217–269.
- (51) Föhlisch, A.; Nyberg, M.; Bennich, P.; Triguero, L.; Hasselström, J.; Karis, O.; Pettersson, L. G. M.; Nilsson, A. The Bonding of CO to Metal Surfaces. J. Chem. Phys. 2000, 112, 1946–1958.
- (52) Föhlisch, A.; Nyberg, M.; Hasselström, J.; Karis, O.; Pettersson, L. G. M.;

- Nilsson, A. How Carbon Monoxide Adsorbs in Different Sites. *Phys. Rev. Lett.* **2000**, *85*, 3309–3312.
- (53) Pettersson, L. G. M.; Nilsson, A. A Molecular Perspective on the d-Band Model: Synergy Between Experiment and Theory. *Top. Cat.* **2014**, *57*, 2–13.
- (54) Sheppard, N.; Nguyen, T. T. In Advances in Infrared and Raman Spectroscopy: v.
  5; Clark, R. J. H., Hester, R. E., Eds.; Heyden, 1978; pp 67–148.
- (55) Gunathunge, C. M.; Ovalle, V. J.; Li, Y.; Janik, M. J.; Waegele, M. M. Existence of an Electrochemically Inert CO Population on Cu Electrodes in Alkaline pH. ACS Catal. 2018, 8, 7507–7516.
- (56) Li, C. W.; Ciston, J.; Kanan, M. W. Electroreduction of Carbon Monoxide to Liquid Fuel on Oxide-Derived Nanocrystalline Copper. *Nature* 2014, 508, 504– 507.
- (57) Manthiram, K.; Beberwyck, B. J.; Alivisatos, A. P. Enhanced Electrochemical Methanation of Carbon Dioxide with a Dispersible Nanoscale Copper Catalyst. J. Am. Chem. Soc. 2014, 136, 13319–13325.
- (58) Hoang, T. T. H.; Ma, S.; Gold, J. I.; Kenis, P. J. A.; Gewirth, A. A. Nanoporous Copper Films by Additive-Controlled Electrodeposition: CO<sub>2</sub> Reduction Catalysis. ACS Catal. 2017, 7, 3313–3321.
- (59) Wang, L.; Nitopi, S.; Wong, A. B.; Snider, J. L.; Nielander, A. C.; Morales-Guio, C. G.; Orazov, M.; Higgins, D. C.; Hahn, C.; Jaramillo, T. F. Electrochemically Converting Carbon Monoxide to Liquid Fuels by Directing Selectivity with Electrode Surface Area. Nat. Catal. 2019, 2, 702–708.
- (60) Gao, D.; Sinev, I.; Scholten, F.; Arán-Ais, R. M.; Divins, N. J.; Kvashnina, K.; Timoshenko, J.; Roldan Cuenya, B.

- Selective CO<sub>2</sub> Electroreduction to Ethylene and Multicarbon Alcohols via Electrolyte-Driven Nanostructuring. *Angew. Chem. Inter. Ed.* **2019**, *58*, 17047–17053.
- (61) Koper, M. T. M.; van Santen, R. A.; Wasileski, S. A.; Weaver, M. J. Field-Dependent Chemisorption of Carbon Monoxide and Nitric Oxide on Platinum-Group (111) Surfaces: Quantum Chemical Calculations Compared with Infrared Spectroscopy at Electrochemical and Vacuum-Based Interfaces. J. Chem. Phys. 2000, 113, 4392–4407.
- (62) Mason, S. E.; Grinberg, I.; Rappe, A. M. Adsorbate-Adsorbate Interactions and Chemisorption at Different Coverages Studied by Accurate ab initio Calculations: CO on Transition Metal Surfaces. J. Phys. Chem. B 2006, 110, 3816–3822.
- (63) Shaw, S.; Berna, A.; Feliu, J.; Nichols, R.; Jacob, T.; Schiffrin, D. Role of Axially Coordinated Surface Sites for Electrochemically Controlled Carbon Monoxide Adsorption on Single Crystal Copper Electrodes. *Phys. Chem. Chem. Phys.* **2011**, *13*, 5242–5251.
- (64) Kim, Y.-G.; Baricuatro, J. H.; Javier, A.; Gregoire, J. M.; Soriaga, M. P. The Evolution of the Polycrystalline Copper Surface, First to Cu(111) and Then to Cu(100), at a Fixed CO<sub>2</sub>RR Potential: A Study by *Operando* EC-STM. *Langmuir* **2014**, 30, 15053–15056.
- (65) Gunathunge, C. M.; Ovalle, V. J.; Waegele, M. M. Probing Promoting Effects of Alkali Cations on the Reduction of CO at the Aqueous Electrolyte/Copper Interface. *Phys. Chem. Chem. Phys.* 2017, 19, 30166–30172.
- (66) Ovalle, V. J.; Waegele, M. M. Impact of Electrolyte Anions on the Adsorption of CO on Cu Electrodes. J. Phys. Chem. C 2020, 124, 14713–14721.

- (67) Varela, A. S.; Ju, W.; Reier, T.; Strasser, P. Tuning the Catalytic Activity and Selectivity of Cu for CO<sub>2</sub> Electroreduction in the Presence of Halides. *ACS Catal.* **2016**, *6*, 2136–2144.
- (68) Resasco, J.; Chen, L. D.; Clark, E.; Tsai, C.; Hahn, C.; Jaramillo, T. F.; Chan, K.; Bell, A. T. Promoter Effects of Alkali Metal Cations on the Electrochemical Reduction of Carbon Dioxide. J. Am. Chem. Soc. 2017, 139, 11277–11287.
- (69) Huang, Y.; Ong, C. W.; Yeo, B. S. Effects of Electrolyte Anions on the Reduction of Carbon Dioxide to Ethylene and Ethanol on Copper (100) and (111) Surfaces. *ChemSusChem* **2018**, *11*, 3299–3306.
- (70) Li, F.; Thevenon, A.; Rosas-A.; Hernández, Wang, Z.; Li. Y.: Gabardo, C. M.; Ozden, A.; Dinh, C. T.; Li, J.; Wang, Y.; Edwards, J. P.; McCallum, C.; Xu, Y.: Tao, L.; Liang, Z.-Q.; Luo, M.; Wang, X.; Li, H.; O'Brien, C. P.; Tan, C.-S.; Nam, D.-H.; Quintero-Bermudez, R.: Zhuang, T.-T.; Li, Y. C.; Han, Z.; Britt, R. D.; Sinton, D.; Agapie, T.; Peters, J. C.; Sargent, E. H. Molecular Tuning of CO<sub>2</sub>-to-Ethylene Conversion. Nature **2020**, *577*, 509–513.
- (71) Pérez-Gallent, E.; Figueiredo, M. C.; Calle-Vallejo, F.; Koper, M. T. M. Spectroscopic Observation of a Hydrogenated CO Dimer Intermediate During CO Reduction on Cu(100) Electrodes. *Angew. Chem. Int. Ed.* **2017**, *56*, 3621–3624.
- (72) Jackman, T. E.; Griffiths, K.;
  Davies, J. A.; Norton, P. R. Absolute
  Coverages and Hysteresis Phenomena
  Associated with the CO-induced Pt(100)
  hex↔(1×1) Phase Transition. J. Chem.
  Phys. 1983, 79, 3529–3533.
- (73) Zou, S.; Gomez, R.; Weaver, M. J. Infrared Spectroscopy of Carbon Monoxide

- at the Ordered Palladium (110)-Aqueous Interface: Evidence for Adsorbate-Induced Surface Reconstruction. *Surf. Sci.* **1998**, *399*, 270–283.
- (74) Blizanac, B. B.; Lucas, C. A.; Gallagher, M. E.; Arenz, M.; Ross, P. N.; Marković, N. M. Anion Adsorption, CO Oxidation, and Oxygen Reduction Reaction on a Au(100) Surface: The pH Effect. J. Phys. Chem. B 2004, 108, 625–634.
- (75) Eren, B.; Zherebetskyy, D.; Patera, L. L.; Wu, C. H.; Bluhm, H.; Africh, C.; Wang, L.-W.; Somorjai, G. A.; Salmeron, M. Activation of Cu(111) Surface by Decomposition into Nanoclusters Driven by CO Adsorption. Science 2016, 351, 475–478.
- (76) Vollmer, S.; Witte, G.; Wöll, C. Determination of Site Specific Adsorption Energies of CO on Copper. *Catal. Lett.* **2001**, 77, 97–101.
- (77) Mason, S. E.; Grinberg, I.; Rappe, A. M. First-Principles Extrapolation Method for Accurate CO Adsorption Energies on Metal Surfaces. *Phys. Rev. B* 2004, 69, 161401.
- (78) Gunathunge, C. M.; Li, J.; Li, X.; Hong, J. J.; Waegele, M. M. Revealing the Predominant Surface Facets of Rough Cu Electrodes under Electrochemical Conditions. *ACS Catal.* **2020**, *10*, 6908–6923.
- (79) Hori, Y.; Koga, O.; Watanabe, Y.; Matsuo, T. FTIR Measurements of Charge Displacement Adsorption of CO on Polyand Single Crystal (100) of Cu Electrodes. *Electrochim. Acta* **1998**, 44, 1389–1395.
- (80) Wuttig, A.; Liu, C.; Peng, Q.; Yaguchi, M.; Hendon, C. H.; Motobayashi, K.; Ye, S.; Osawa, M.; Surendranath, Y. Tracking a Common Surface-Bound Intermediate during

- $CO_2$ -to-Fuels Catalysis. *ACS Cent. Sci.* **2016**,  $\mathcal{Z}$ , 522–528.
- (81) Schouten, K. J. P.; Pérez Gallent, E.; Koper, M. T. M. The Influence of pH on the Reduction of CO and CO<sub>2</sub> to Hydrocarbons on Copper Electrodes. *J. Electroanal. Chem.* **2014**, *716*, 53–57.
- (82) Hollins, P.; Pritchard, J. Infrared Studies of Chemisorbed Layers on Single Crystals. *Prog. Surf. Sci.* **1985**, *19*, 275–349.
- (83) Persson, B. N. J.; Ryberg, R. Vibrational Phase Relaxation at Surfaces: CO on Ni(111). *Phys. Rev. Lett.* **1985**, *54*, 2119–2122.
- (84) Borguet, E.; Dai, H.-L. Site-Specific Properties and Dynamical Dipole Coupling of CO Molecules Adsorbed on a Vicinal Cu(100) Surface. *J. Chem. Phys.* **1994**, *101*, 9080–9095.
- (85) Hamm, P.; Lim, M.; Hochstrasser, R. M. Structure of the Amide I Band of Peptides Measured by Femtosecond Nonlinear-Infrared Spectroscopy. *J. Phys. Chem. B* **1998**, *102*, 6123–6138.
- (86) Chang, S. C.; Weaver, M. J. In Situ Infrared Spectroscopy of Carbon Monoxide Adsorbed at Ordered Platinum (100)—Aqueous Interfaces: Double-Layer Effects upon the Adsorbate Binding Geometry. J. Phys. Chem. 1990, 94, 5095—5102.
- (87) Woodruff, D.; Hayden, B.; Prince, K.; Bradshaw, A. Dipole Coupling and Chemical Shifts in IRAS of CO Adsorbed on Cu(110). Surf. Sci. 1982, 123, 397–412.
- (88) Koga, O.; Teruya, S.; Matsuda, K.; Minami, M.; Hoshi, N.; Hori, Y. Infrared Spectroscopic and Voltammetric Study of Adsorbed CO on Stepped Surfaces of Copper Monocrystalline Electrodes. *Electrochim. Acta* **2005**, *50*, 2475–2485.

- (89) Borguet, E.; Dai, H.-L. Probing Surface Short Range Order and Inter-Adsorbate Interactions through IR Vibrational Spectroscopy: CO on Cu(100). J. Phys. Chem. B 2005, 109, 8509–8512.
- (90) Malkani, A. S.; Li, J.; Anibal, J.; Lu, Q.; Xu, B. Impact of Forced Convection on Spectroscopic Observations of the Electrochemical CO Reduction Reaction. ACS Catal. 2020, 10, 941–946.
- (91) Tüshaus, M.; Schweizer, E.; Hollins, P.; Bradshaw, A. Yet Another Vibrational Study of the Adsorption System Pt111-CO. J. Electron Spectrosc. Relat. Phenom. 1987, 44, 305–316.
- (92) Fuggle, J.; Menzel, D. Coverage Dependent Shifts of XPS Peaks During Chemisorption on Metals. Surf. Sci. 1975, 53, 21–34.
- (93) Hammer, B. Coverage Dependence of N<sub>2</sub> Dissociation at an N, O, or H Precovered Ru(0001) Surface Investigated with Density Functional Theory. *Phys. Rev. B* **2001**, *63*, 205423.
- (94) Miller, S. D.; Kitchin, J. R. Relating the Coverage Dependence of Oxygen Adsorption on Au and Pt fcc(111) Surfaces Through Adsorbate-Induced Surface Electronic Structure Effects. Surf. Sci. 2009, 603, 794–801.
- (95) Garfunkel, E. L.; Crowell, J. E.; Somorjai, G. A. The Strong Influence of Potassium on the Adsorption of Carbon Monoxide on Platinum Surfaces: a TDS and HREELS Study. J. Phys. Chem. 1982, 86, 310–313.
- (96) Rodriguez, J. A.; Campbell, C. T. Quantum Chemical Studies of the Effects of Electron-Transferring Ligands Upon Carbon Monoxide Chemisorption on Copper(100). J. Phys. Chem. 1987, 91, 2161–2171.

- (97) Mortensen, J.; Hammer, B.; Nørskov, J. A Theoretical Study of Adsorbate-Adsorbate Interactions on Ru(0001). Surf. Sci. 1998, 414, 315–329.
- (98) Kiskinova, M.; Goodman, D. Modification of Chemisorption Properties by Electronegative Adatoms: H<sub>2</sub> and CO on Chlorided, Sulfided, and Phosphided Ni(100). Surf. Sci. **1981**, 108, 64–76.
- (99) Gorin, C. F.; Beh, E. S.; Kanan, M. W. An Electric Field-Induced Change in the Selectivity of a Metal Oxide-Catalyzed Epoxide Rearrangement. J. Am. Chem. Soc. **2012**, 134, 186–189.
- (100) Ledezma-Yanez, I.; Wallace, W. D. Z.; Sebastián-Pascual, P.; Climent, V.; Feliu, J. M.; Koper, M. T. M. Interfacial Water Reorganization as a pH-Dependent Descriptor of the Hydrogen Evolution Rate on Platinum Electrodes. *Nat. Energy* **2017**, *2*, 17031.
- (101) Bagger, A.; Arnarson, L.; Hansen, M. H.; Spohr, E.; Rossmeisl, J. Electrochemical CO Reduction: A Property of the Electrochemical Interface. J. Am. Chem. Soc. 2019, 141, 1506–1514.
- (102) Banerjee, S.; Han, X.; Thoi, V. S. Modulating the Electrode-Electrolyte Interface with Cationic Surfactants in Carbon Dioxide Reduction. *ACS Catal.* **2019**, *9*, 5631–5637.
- (103) Sorenson, S. A.; Patrow, J. G.; Dawlaty, J. M. Solvation Reaction Field at the Interface Measured by Vibrational Sum Frequency Generation Spectroscopy. J. Am. Chem. Soc. 2017, 139, 2369–2378.
- (104) Patrow, J. G.; Sorenson, S. A.; Dawlaty, J. M. Direct Spectroscopic Measurement of Interfacial Electric Fields near an Electrode under Polarizing or Current-Carrying Conditions. J. Phys. Chem. C 2017, 121, 11585–11592.

- (105) Ge, A.; Videla, P. E.; Lee, G. L.; Rudshteyn, B.; Song, J.; Kubiak, C. P.; Batista, V. S.; Lian, T. Interfacial Structure and Electric Field Probed by in Situ Electrochemical Vibrational Stark Effect Spectroscopy and Computational Modeling. J. Phys. Chem. C 2017, 121, 18674–18682.
- (106) Clark, M. L.; Ge, A.; Videla, P. E.; Rudshteyn, B.; Miller, C. J.; Song, J.; Batista, V. S.; Lian, T.; Kubiak, C. P. CO<sub>2</sub> Reduction Catalysts on Gold Electrode Surfaces Influenced by Large Electric Fields. J. Am. Chem. Soc. 2018, 140, 17643–17655.
- (107) Sarkar, S.; Maitra, A.; Banerjee, S.; Thoi, V. S.; Dawlaty, J. M. Electric Fields at Metal-Surfactant Interfaces: A Combined Vibrational Spectroscopy and Capacitance Study. J. Phys. Chem. B 2020, 124, 1311–1321.
- (108) Lambert, D. K. Vibrational Stark Effect of CO on Ni(100), and CO in the Aqueous Double Layer: Experiment, Theory, and Models. J. Chem. Phys. 1988, 89, 3847–3860.
- (109) Fried, S. D.; Boxer, S. G. Measuring Electric Fields and Noncovalent Interactions Using the Vibrational Stark Effect. *Acc. Chem. Res.* **2015**, *48*, 998–1006.
- (110) Magnussen, O. M.; Groß, A. Toward an Atomic-Scale Understanding of Electrochemical Interface Structure and Dynamics. J. Am. Chem. Soc. **2019**, 141, 4777–4790.
- (111) Pennathur, A. K.; Voegtle, M. J.; Menachekanian, S.; Dawlaty, J. M. Strong Propensity of Ionic Liquids in Their Aqueous Solutions for an Organic-Modified Metal Surface. The Journal of Physical Chemistry B 2020, 124, 7500– 7507.
- (112) Hussain, G.; Pérez-Martínez, L.; Le, J.-B.; Papasizza, M.; Cabello, G.;

- Cheng, J.; Cuesta, A. How Cations Determine the Interfacial Potential Profile: Relevance for the CO<sub>2</sub> Reduction Reaction. *Electrochim. Acta* **2019**, *327*, 135055.
- (113) Iijima, G.; Inomata, T.; Yamaguchi, H.; Ito, M.; Masuda, H. Role of a Hydroxide Layer on Cu Electrodes in Electrochemical CO<sub>2</sub> Reduction. *ACS Catal.* **2019**, *9*, 6305–6319.
- (114) Dunwell, M.; Yang, X.; Setzler, B. P.; Anibal, J.; Yan, Y.; Xu, B. Examination of Near-Electrode Concentration Gradients and Kinetic Impacts on the Electrochemical Reduction of CO<sub>2</sub> using Surface-Enhanced Infrared Spectroscopy. ACS Catal. 2018, 8, 3999–4008.
- (115) Dunwell, M.; Yang, X.; Yan, Y.; Xu, B. Potential Routes and Mitigation Strategies for Contamination in Interfacial Specific Infrared Spectroelectrochemical Studies. J. Phys. Chem. C 2018, 122, 24658–24664.
- (116) Heinen, M.; Chen, Y.; Jusys, Z.; Behm, R. In Situ ATR-FTIRS Coupled with On-Line DEMS under Controlled Mass Transport Conditions - A Novel Tool for Electrocatalytic Reaction Studies. *Electrochim. Acta* 2007, 52, 5634– 5643.
- (117) Chen, L. D.; Urushihara, M.; Chan, K.; Nørskov, J. K. Electric Field Effects in Electrochemical CO<sub>2</sub> Reduction. *ACS Catal.* **2016**, *6*, 7133–7139.
- (118) Li, X.; Gunathunge, C. M.; Agrawal, N.; Montalvo-Castro, H.; Jin, J.; Janik, M. J.; Waegele, M. M. Impact of Alkali Metal Cations and Iron Impurities on the Evolution of Hydrogen on Cu Electrodes in Alkaline Electrolytes. J. Electrochem. Soc. 2020, 167, 106505.
- (119) Piontek, S. M.; DelloStritto, M.; Mandal, B.; Marshall, T.; Klein, M. L.;

Borguet, E. Probing Heterogeneous Charge Distributions at the  $\alpha$ -Al<sub>2</sub>O<sub>3</sub>(0001)/H<sub>2</sub>O Interface. *J. Am. Chem. Soc.* **2020**, *142*, 12096–12105.

## Graphical TOC Entry

